International Journal of Thermophysics (2022) 43:41
https://doi.org/10.1007/s10765-021-02961-3

TALGAT KHASANSHIN: IN MEMORIAM

A Fundamental Equation of State for Chloroethene for Temperatures from the Triple Point to 430 K and Pressures to 100 MPa

Monika Thol[1] · Florian Fenkl[1] · Eric W. Lemmon[2]

Received: 9 November 2021 / Accepted: 8 December 2021 / Published online: 10 January 2022

Abstract
A fundamental equation of state in terms of the Helmholtz energy is presented for chloroethene (vinyl chloride). Due to its fundamental nature, it can be used to consistently calculate all thermodynamic state properties in the fluid region. Based on the underlying experimental database, it is valid from the triple-point temperature 119.31 K to 430 K with a maximum pressure of 100 MPa. In addition to the accurate reproduction of experimental data, correct extrapolation behavior during the development of the equation was attained. This enables the equation to be applied in modern mixture frameworks.

Keywords Equation of state · Helmholtz energy · Thermodynamic properties · Vinyl chloride

1 Introduction

One of the most important synthetic polymers in industry is polyvinyl chloride (PVC). Its applications range from pipes and packaging to cable insulation, clothing, heath care, and vinyl records, as well as many other things in daily life.

In the chemical industry, the monomeric chemical substance vinyl chloride is used as a precursor for PVC, thus making it "one of the most important commodity chemicals" [1]. Vinyl chloride is also known as chloroethene, monochloroethylene, or ethylene monochloride and has the CAS number 75-01-4. As all names imply, vinyl chloride is an organochloride and as such consists of carbon and at least one

This article is part of the Special Issue in Memory of Professor Talgat Khasanshin.

✉ Monika Thol
m.thol@thermo.rub.de

[1] Thermodynamics, Ruhr-Universität Bochum, Universitätsstraße 150, 44801 Bochum, Germany

[2] Applied Chemicals and Materials Division, National Institute of Standards and Technology, Boulder, CO, USA

chlorine atom. Specifically, covalent bonds surround the vinyl group, i.e., one chlorine, two carbon, and three hydrogen atoms.

Under standard conditions, vinyl chloride is a volatile, colorless gas. It has a high solubility in all organic solvents, but is barely soluble in water. Furthermore, its sweet odor can only be sensed at a threshold of 3000 ppm, far above the safety threshold or action level of 1 ppm to 5 ppm as regulated by OSHA [2]. It is highly flammable, potentially explosive, toxic, and carcinogenic. The latter was discovered after many workers suffered from the "vinyl chloride illness" after being exposed to high levels of the substance [3]. Apart from carbon dioxide, thermal decomposition of vinyl chloride can form toxic products, i.e., carbon monoxide, hydrogen chloride, and phosgene depending on the availability of oxygen [4]. Since its gaseous density is higher than that of air, vinyl chloride will stay close to the ground and can travel significant distances. If not contained and mixed with air, it can cause fires or health hazards. Therefore, safe storage and transport requires pressurized containers. In its gaseous state, it is rather unstable and known to spontaneously polymerize into PVC. The polymer, however, is very stable and storable as flakes or pellets. As a positive side effect, PVC loses the acute toxicity of the monomer. While the polymerization of vinyl chloride is the desired outcome of its use, a premature polymerization can disrupt the entire production process and must be avoided. Rapid polymerization is caused by heat and the presence of oxygen and light. If oxygen or another common oxidizing agent is unavailable, metals like aluminum and copper can also be used as a catalyst [1].

While vinyl chloride can be produced via several routes, the economically feasible methods on an industrial scale are the hydrochlorination of acetylene and the dehydrochlorination, i.e., thermal cracking, of 1,2-dichloroethane. The former method is mainly employed in China, where large coal reserves provide a cheap and vast supply of acetylene [1]. Nevertheless, the industrially most common production method of vinyl chloride is the thermal cracking of 1,2-dichloroethane.

As the basic material for one of the most important plastic products, industrial stakeholders rely upon a user-friendly, cost-effective, and scientifically sound approximation of the thermodynamic properties of vinyl chloride, as well as the educts and products involved in the reactions. This work, combined with the development and publication of equations of state for acetylene [5, 6], hydrogen chloride [7], 1,2-dichloroethane [8], and chlorine [9], provides a complete set of tools to industry for the substances involved in the production of vinyl chloride. The thermodynamic state properties available in this set come through the application of fundamental equations of state in terms of the Helmholtz energy. These equations are mainly of empirical nature and, therefore, include numerous adjustable parameters. In order to predict the fluid's thermodynamic properties as accurately as possible, the determination of these parameters requires comprehensive and high-quality experimental measurements. If conscientiously conducted, these laboratory experiments are complex and time-consuming. Furthermore, challenging characteristics such as flammability, toxicity, or corrosiveness complicate the measurements. One of the biggest challenges for the development of equations of state for fluids, which are important for the chemical industry, is the available database. In order to mitigate these disadvantages, much effort has been put in the

optimization of the fitting algorithm proposed by Lemmon and Jacobsen in 2005 [10]. As a result, Lemmon [11] designed a non-linear fitting algorithm that enables not only the use of experimental measurements but also the formulation of suitable boundary conditions in regions where data are not available. This offers the possibility of developing fundamental equations of state based on very limited databases. The minimum information required is vapor pressure, homogeneous density, and a caloric property, preferably speed of sound. Additional properties are always helpful, but not mandatory.

Over the last few years, the fitting algorithm, as well as new measurements on density and speed of sound were used in the development of equations of state for the aforementioned components involved in the reactions [5, 7–9]. Similar to these fluids, the database for vinyl chloride is rather poor. In addition to the challenging characteristics of the fluid, this might be due to the nearly exclusive application in the PVC production and, thus, low scientific attention. Only industry is interested in this fluid, which usually does not have the infrastructure to measure thermodynamic properties. Most publications feature vinyl chloride merely in a mixture with another component in a restricted temperature and pressure range.

Javed et al. [12], therefore, recently carried out density and speed-of-sound measurements of vinyl chloride, which are the basis for the equation of state presented in this work. Prior to this publication, there were no data for the speed of sound available. In terms of density, the authors investigated a more comprehensive pressure range than previously covered; thus increasing the range of validity of the present equation of state.

2 The Helmholtz Equation of State

The equation of state for vinyl chloride is formulated in terms of the Helmholtz energy as a function of temperature and density, *cf.* Equation (1). Due to its fundamental nature, it can be used to calculate all thermodynamic properties from one mathematical expression and its derivatives with respect to the independent variables.

$$\alpha(\tau,\delta) = \frac{a(T,\rho)}{RT} = \frac{a^{\mathrm{o}}(T,\rho) + a^{\mathrm{r}}(T,\rho)}{RT} = \alpha^{\mathrm{o}}(\tau,\delta) + \alpha^{\mathrm{r}}(\tau,\delta), \tag{1}$$

For practical reasons, the Helmholtz energy a is reduced by the temperature and the universal gas constant. The dimensionless Helmholtz energy α is subdivided into ideal (superscript o) and residual (superscript r) parts. For simplification, the independent variables are reduced by their values at the critical point:

$$\tau = \frac{T_{\mathrm{c}}}{T} \tag{2}$$

and

$$\delta = \frac{\rho}{\rho_c}. \tag{3}$$

The ideal part is based on theoretical considerations from kinetic gas theory. It combines the intramolecular forces based on the concept of the degrees of freedom of an ideal gas. Although the theory has been comprehensively investigated and the modes of motion as well as the corresponding temperatures could be measured, it is highly complex. Since the purpose of the present equation of state is the accurate description of real fluid properties, the simplified concept of a rigid rotator, harmonic oscillator as proposed by Span [13] is adopted. It is expressed in terms of the isobaric heat capacity of the ideal gas as a function of temperature:

$$\frac{c_p^o}{R} = c_0 + \sum_{i=1}^{I_{PE}} m_i \frac{\left(u_i/T\right)^2 \exp\left(u_i/T\right)}{\left[\exp\left(u_i/T\right) - 1\right]^2}. \tag{4}$$

Contributions from translation, rotation, and vibration are considered for the heat capacity of the ideal gas. For most fluids, translation and rotation can always be treated as fully excited, even at very low temperatures. Their degrees of freedom are, thus, summarized in the temperature-independent part

$$c_0 = \frac{\nu}{2} + 1 = \frac{\nu_{trans} + \nu_{rot}}{2} + 1 \tag{5}$$

With vinyl chloride being a non-linear molecule, $\nu = 3$ for both translation (trans) and rotation (rot). The vibrational modes are dependent on temperature and are calculated with an exponential function, the so-called Planck–Einstein terms (subscript PE, *cf*. Eq. 4). Although based on theory, they are treated empirically, which not only reduces the number of required terms but also compensates for contributions from the kinetic gas theory not taken into account due to the simplified approach (such as anharmonicity). The equation for the isobaric heat capacity of the ideal gas is made dimensionless by reducing with the critical temperature ($\tau = T_c/T$) and switching to the isochoric heat capacity according to $c_v^o = c_p^o - R$. With the relation

$$a^o(T,\rho) = u^o(T) - Ts^o(T,\rho) = u_0^o - Ts_0^o + \int_{T_0}^{T} c_v^o \mathrm{d}T - T\int_{T_0}^{T} \frac{c_v^o}{T}\mathrm{d}T + RT\ln\left(\frac{\rho}{\rho_0}\right), \tag{6}$$

the ideal part of the reduced Helmholtz energy results in

$$\alpha^o = \ln\delta + \left(c_0 - 1\right)\ln\tau + c^{II} + c^I\tau + \sum_{i=1}^{I_{PE}} m_i \ln\left[1 - \exp\left(-u_i\tau/T_c\right)\right] \tag{7}$$

with $\tau = T_c/T$ and $\delta = \rho/\rho_c$. The integration constants c^I and c^{II} were adjusted so that the molar enthalpy h_0 and molar entropy s_0 are both equal to zero for the saturated liquid at the normal boiling point. The corresponding parameters are listed in Table 1.

Table 1 Parameters of the ideal part of the reduced Helmholtz energy according to Eq. 7

i	m	u (K)
1	4.51	923
2	4.45	1907
3	3.04	4400
c_0	4	
c^{I}	3.6032015766362435	
c^{II}	−3.4387095412593389	

Table 2 Parameters of the residual part of the reduced Helmholtz energy according to Eq. 8

i	n_i	t_i	d_i	l_i	η_i	β_i	γ_i	ε_i
1	0.012261627	1	4					
2	0.8604231	0.136	1					
3	−1.0169596	0.984	1					
4	−0.81353519	1.02	2					
5	0.23529717	0.624	3					
6	−0.87520652	1.215	1	2				
7	−1.0092224	1.427	3	2				
8	0.51890592	0.9	2	1				
9	−0.15911867	4	2	2				
10	−0.007640016	0.6	7	1				
11	−0.22858771	3.45	1	3				
12	0.9093646	1.42	1		1.736	0.77	1.3	0.82
13	−0.19999899	0.9	2		30	815	1.1	0.92
14	−0.37519445	1.475	1		2.425	0.77	1.59	0.995
15	0.97421121	0.5	1		0.714	0.41	1.5	0.71
16	−1.006613	1.156	1		0.694	0.32	0.93	0.66

The residual part of the reduced Helmholtz energy is empirically determined. It is a combination of three types of terms, i.e., polynomial-like, exponential, and Gaussian bell-shaped terms. In general, the first two types are sufficient to accurately describe the entire fluid surface. To better characterize the critical region, Gaussian bell-shaped terms are used. In the case of vinyl chloride, 5 polynomial-like, 6 exponential, and 5 Gaussian bell-shaped terms are employed:

$$\alpha^{\mathrm{r}}(\delta,\tau)=\sum_{i=1}^{5} n_i\delta^{d_i}\tau^{t_i}+\sum_{i=6}^{11} n_i\delta^{d_i}\tau^{t_i}\exp\left(-\delta^{l_i}\right)+\sum_{i=12}^{16} n_i\delta^{d_i}\tau^{t_i}\exp\left[-\eta_i\left(\delta-\varepsilon_i\right)^2-\beta_i\left(\tau-\gamma_i\right)^2\right]. \tag{8}$$

The corresponding parameters are listed in Table 2.

Some characteristic thermodynamic properties of vinyl chloride, which are important for the equation of state, are summarized in Table 3.

All thermodynamic state properties can be calculated from the Helmholtz energy and its derivatives with respect to the natural variables of temperature and density.

Table 3 Thermodynamic properties of vinyl chloride and the universal gas constant

Property	Value	Reference
T_c	425.0 K	[14]
ρ_c	5.65 mol·dm^{-3}	[14]
p_c	5.6003 MPa	This work
T_{NBP}	259.26 K	This work
$\rho_{NBP,liq}$	15.522 mol·dm^{-3}	This work
T_{tr}	119.31 K	[15]
$\rho_{tr,liq}$	19.699 mol·dm^{-3}	This work
p_{tr}	0.0000404 kPa	This work
ω	0.160	This work
M	62.49822 g·mol^{-1}	[16]
R	8.314462618 J·mol^{-1}·K^{-1}	[17]

tr refers to the triple-point, *NBP* to the normal boiling point

This is also valid for vapor–liquid-equilibrium properties. However, in order to determine the temperature and density at saturation, the Maxwell criterion [18, 19] (thermal, mechanical, and chemical equilibrium of both phases) has to be solved iteratively. For the reduction of computation time, ancillary equations for the vapor pressure and saturation densities were developed:

$$\ln\left(\frac{p_v}{p_c}\right) = \left(\frac{T_c}{T}\right)\sum_{i=1}^{5} n_i\left(1-\frac{T}{T_c}\right)^{t_i}, \tag{9}$$

$$\frac{\rho'}{\rho_c} = 1 + \sum_{i=1}^{6} n_i\left(1-\frac{T}{T_c}\right)^{t_i}, \tag{10}$$

and

$$\ln\left(\frac{\rho''}{\rho_c}\right) = \sum_{i=1}^{6} n_i\left(1-\frac{T}{T_c}\right)^{t_i}. \tag{11}$$

The corresponding parameters are listed in Table 4. Deviations from the actual Helmholtz energy equation of state are presented in Fig. 1. These equations can be used to quickly calculate accurate starting values for the iterative procedure. However, for the calculation of real property data, the fundamental equation of state should be used.

Test values for computer implementations are given in Table 5. The number of digits does not refer to the uncertainty of calculated data, but allows numerical validation of the implementation of the EOS.

Table 4 Parameters of the ancillary equations for pressure p_v, saturated liquid density ρ', and saturated vapor density ρ''

i	Vapor pressure, Eq. 9		Saturated liquid density, Eq. 10		Saturated vapor density, Eq. 11	
	n_i	t_i	n_i	t_i	n_i	t_i
1	−6.945	1	1.8041	0.33	−0.5868	0.193
2	1.7737	1.5	5.629	1.19	−5.3182	0.687
3	−2.0553	2.78	−18.450	1.75	−14.6323	2.540
4	−2.813	5.2	33.235	2.39	−46.665	6.12
5	−2.756	15	−66.136	3.22	−98.3277	13.0
6			47.53	3.46	−228.973	25.5

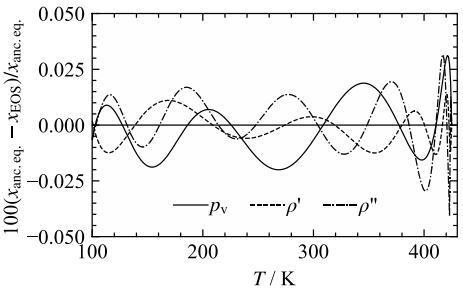

Fig. 1 Percentage deviations between the ancillary equations for vapor pressure p_v, saturated liquid density ρ', and saturated vapor density ρ'' and the equation of state

3 Range of Validity and Critical Parameters

The database, which was available for the development of the present equation of state, is rather restricted. The equation is mainly based on very recent density and speed of sound measurements of Javed et al. [12]. Other than these, only limited experimental data are available in the literature. Most publications feature vinyl chloride merely in a mixture with another component over limited temperature and pressure ranges. Since the aim of this work was to develop a pure-fluid equation, only a few of the data points from these publications can be used. Although the vapor pressure has the broadest experimental coverage, most of the publications provide less than five data points each.

However, the data of Javed et al. [12], combined with vapor pressures from other researchers, were sufficient to develop the present equation of state. Nevertheless, the user should be aware of the limited range of validity and possibly higher uncertainties for properties such as heat capacities or heats of vaporization, which have not been experimentally investigated.

An overview of the data situation is illustrated in Fig. 2. The range of validity is usually defined based on the experimental data. For vinyl chloride, experimental data are only available down to 190 K (gray-shaded area in Fig. 2), which is significantly higher than the triple-point temperature $T_{tr} = 119.31$ K [15]. However, the triple-point temperature is still chosen as the lower temperature limit of the present equation of state because it reliably extrapolates down to very low temperatures as shown in Sect. 5.

Table 5 Test values for verification of computer implementations

T (K)	ρ (mol·dm^{-3})	p (MPa)	w (m·s^{-1})	c_p (J·mol^{-1}·K^{-1})	h (J·mol^{-1})	s (J·mol^{-1}·K^{-1})	a (J·mol^{-1})
250	0.03	0.0611336026	198.051441	49.1470240	21,830.1713	88.2755532	−2276.50376
250	16	10.5895545	1155.49169	91.1392445	−477.949658	−4.48949199	−17.4238160
300	0.18	0.413797863	204.981105	59.5414183	23,878.6868	80.5342776	−2580.47364
300	15	23.0374719	1008.04450	91.4066946	4518.73773	10.8027936	−257.931823
430	14	88.2661442	982.983659	92.7700338	18,735.1820	37.6281054	−3749.62785

The upper temperature limit of 430 K is slightly above the critical temperature. The information on the critical point is also very limited. Cullick and Ely [14] applied three different estimation approaches based on the corresponding states principle. These methods yield critical temperatures between 420.3 K and 425.6 K. Based on comparisons with results from the approach of Ambrose [20, 21] and Reid et al. [22], Cullick and Ely [14] chose 425 K as the critical temperature with an uncertainty of 5 K. Another estimation of $T_c = 428.96$ K was published by Zernov et al. [23]. During the development of the present equation of state, both critical temperatures were tested. A more accurate representation of the available experimental data was obtained with a value of 425 K used here as the critical temperature. However, the uncertainty of 5 K is rather high, and new measurements would be beneficial. Additionally, the critical density of Cullick and Ely [14] was taken as the starting point for the fit and slightly adjusted to match the experimental data within their experimental uncertainty. The critical pressure calculated from the present equation of state agrees well with the value of Cullick and Ely [14] ($p_c = 5.54$ MPa). The final values applied in this work are listed in Table 3.

The upper limit of the equation in terms of pressure is 100 MPa, and can be extrapolated to 200 MPa with minimal loss in accuracy. The maximum density is 19.7 mol·dm^{-3}, which is the saturated liquid density at the triple-point temperature, *cf*. Table 3.

4 Comparison of the Equation of State to Experimental Data

The quality of equations of state is assessed by comparing values calculated from the equation with experimental data. In this section, percentage deviations as calculated with Eq. 12 are illustrated in the figures.

$$X = 100\left(x_{\mathrm{DATA}} - x_{\mathrm{EOS}}\right)/x_{\mathrm{DATA}}. \tag{12}$$

Average absolute relative deviations (AARD) are presented for each dataset in Tables 6 and 7. The AARD is defined as

$$\mathrm{AARD} = \frac{1}{N}\sum_{i=1}^{N}|X_i|, \tag{13}$$

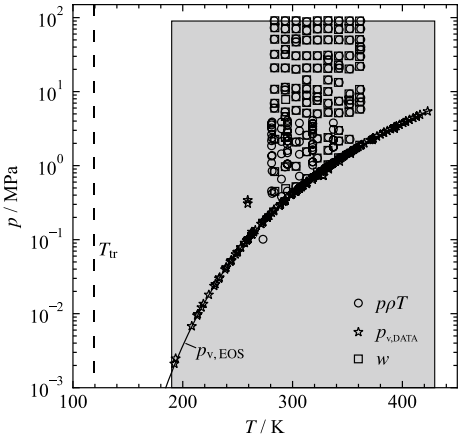

Fig. 2 p,T-diagram including available experimental data. The gray area marks the range where experimental data are available

with N being the number of data points.

Thermal vapor–liquid-equilibrium data are separated into three temperature ranges as indicated in the footnote of Table 6. Homogeneous density and speed-of-sound data are grouped into vapor ($\rho < \rho''$) and liquid ($\rho > \rho'$).

4.1 Isobaric Heat Capacity of the Ideal Gas

There are four datasets available for the isobaric heat capacity of the ideal gas. All of them cover a temperature range from approximately 270 K to 500 K. Only Richards [55] evaluated temperatures up to 1500 K. At low temperatures, three different trends in the data can be observed, *cf*. Figure 3. The data of Gullikson and Nielsen [53] match the data of Richards [55]. The latter were calculated with the fundamental constants given by Birge [57] and by applying the method of Hirschfelder [58], whereas Gullikson and Nielsen [53] calculated the ideal-gas heat capacities from their spectroscopic measurements. The data of Lacher et al. [54] were calculated from information given by Thompson and Torkington [59]. These data are scattered around the results of Gullikson and Nielsen [53] and Richards [55]. The data of Senftleben [56] exhibit a significantly contrary trend when compared to the other data (−1 % to 6 % with increasing temperatures) although the author claims an uncertainty of 2 %. However, fitting either the data of Lacher et al. [54] or the data of Senftleben [56] caused a detoriation in the representation of the accurate speed-of-sound data of Javed et al. [12] Therefore, the data of Richards [55] were chosen here, which are represented within 0.1 %, except for one outlier at 900 K.

4.2 Vapor Pressure

The vapor pressure is the most comprehensively investigated property of this fluid due to several experimental campaigns on vapor–liquid-equilibrium properties of mixtures with vinyl chloride. There are ten datasets comprising more than four state points. However, these data are significantly scattered as illustrated in Fig. 4

Table 6 Average absolute relative deviations AARD of experimental vapor–liquid-equilibrium data calculated with the present equation of state, where N is the number of data points

Author	Ref	N	(T_{min}–T_{max}) (K)	AARD (%)			
				LT[a]	MT[a]	HT[a]	Overall
Vapor pressure p_v							
Carra and Beltrame (1961)	[24]	1	352.22	–	0.23	–	0.23
Dana et al. (1927)	[25]	17	244–334	0.22	0.32	–	0.30
de Loos et al. (1983)	[26]	16	273–424	–	0.93	0.26	0.88
Dreisbach and Shrader (1949)	[27]	3	239–260	0.19	0.83	–	0.41
Giles and Wilson (2006)	[28]	2	273–314	–	0.57	–	0.57
Gillespie et al. (1985)	[29]	3	192–267	7.2	0.50	–	5.0
Gillespie et al. (1985)	[30]	4	259–340	–	0.55	–	0.55
Haccuria and Mathieu (1967)	[31]	21	213–329	0.66	3.6	–	2.3
Hannaert et al. (1967)	[32]	3	213–254	1.0	–	–	1.0
Hirata and Suda (1968)	[33]	2	273–274	–	0.73	–	0.73
Hirata et al. (1966)	[34]	76	299–417	–	0.77	–	0.77
Hradetzky et al. (1976)	[35]	1	293.14	–	2.0	–	2.0
Kovac and Dykyj (1971)	[36]	9	277–334	–	0.36	–	0.36
Lebedev et al. (1967)	[15]	1	259.51	–	1.0	–	1.0
Lim et al. (1997)	[37]	2	303–324	–	4.2	–	4.2
McDonald et al. (1959)	[38]	7	208–261	0.53	0.40	–	0.47
Owens et al. (1987)	[39]	8	293–374	–	1.2	–	1.2
Pearson and McConnell (1975)	[40]	1	293.14	–	10	–	10
Pelnar (1960)	[41]	1	259.26	–	70	–	70
Preuss and Moerke (1987)	[42]	3	303–344	–	0.39	–	0.39
Preuss and Moerke (1987)	[43]	3	293–354	–	1.2	–	1.2
Preuss and Moerke (1988)	[44]	30	263–374	–	0.34	–	0.34
Preuss and Roscher (1973)	[45]	4	263–324	–	2.2	–	2.2
Rozlovskaya and Temkin (1946)	[46]	7	283–344	–	5.0	–	5
Zerfa and Brooks (1996)	[47]	1	328.15	–	21	–	21
Zernov et al. (1978)	[23]	6	293–394	–	5.9	–	5.9
Saturated liquid density ρ'							
Dana et al. (1927)	[25]	7	260–334	–	0.18	–	0.18
de Loos et al. (1983)	[26]	16	273–424	–	1.7	0.68	1.6
Hannaert et al. (1967)	[32]	2	213–234	0.12	–	–	0.12
Mizutani and Yamashita (1950)	[48]	27	222–259	0.17	0.30	–	0.19
Zerfa and Brooks (1996)	[47]	1	328.15	–	0.029	–	0.029
Saturated vapor density ρ''							
Zernov et al. (1978)	[23]	6	293–394	–	3.3	–	3.3

[a]LT: $T/Tc < 0.6$; MT: $0.6 \leq T/Tc \leq 0.98$; HT: $T/Tc > 0.98$

Table 7 Average absolute relative deviations AARD of experimental data for homogeneous densities and caloric data calculated with the present equation of state, where N is the number of data points

Author	Ref	N	$(T_{min}–T_{max})$ (K)	$(p_{min}–p_{max})$(MPa)	AARD (%)	
					Vapor	Liquid
Homogeneous density $p\rho T$						
Cullick and Ely (1982)	[14]	69	280–338	0.4–4.1	–	0.18
Hayduk and Laudie (1974)	[49]	1	273.15	0.101325	0.06	–
Javed et al. (2020)	[12]	105	283–363	0.4–91.1	–	0.046
Speed of sound w						
Javed et al. (2020)	[12]	117	283–362	0.5–91.1	–	0.032
Isobaric heat capacity c_p						
Senftleben (1953)	[50]	1	303.13	0.101325		8.7
Heat of vaporization Δh_{vap}						
Joshi and Zwolinski (1965)	[51]	1	298.14	p_v	1.8	–
Danov and Golubev (1967)	[52]	1	286.54	p_v	8.4	–
Ideal gas heat capacity c_p^o						
Gullikson and Nielsen (1957)	[53]	5	273–501	$\rightarrow 0$	0.099	
Lacher et al. (1956)	[54]	5	297–601	$\rightarrow 0$	0.83	
Richards (1948)	[55]	18	291–1500	$\rightarrow 0$	0.061	
Senftleben (1964)	[56]	5	298–474	$\rightarrow 0$	2.6	

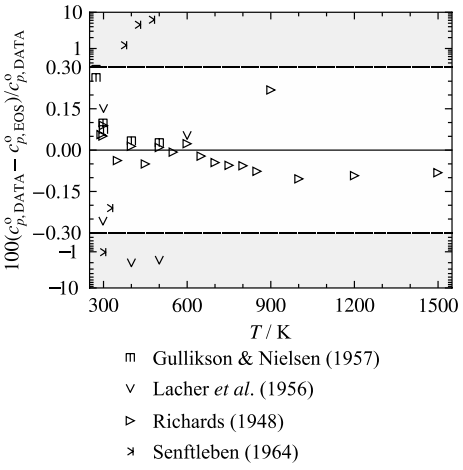

Fig. 3 Percentage deviations of the isobaric heat capacity data of the ideal gas from the equation of state. The y-axis is separated into a linear scale (white background) and a logarithmic scale (gray-shaded area)

(top panel), which makes the choice of the data to be fitted difficult. Since Hirata et al. [34] and Haccuria and Mathieu [31] measured many state points, these are eye catching in the plot. Therefore, these data are deleted from the plot in the bottom panel. Between 250 K and 350 K, the equation was fitted so that it runs through the middle of the data of Dana et al. [25], Preuss and Moerke [44], and Kovac and Dykyj [36]. Most of the remaining data are consistent with each other but are

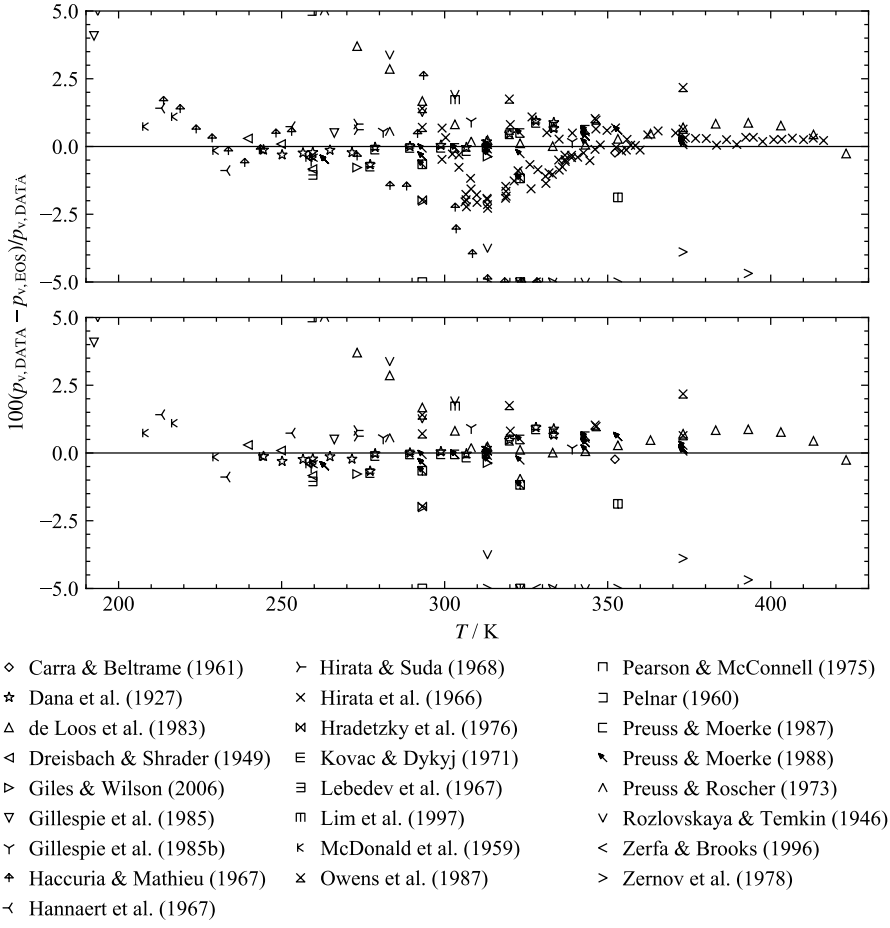

Fig. 4 Percentage deviations of the experimental vapor-pressure data from the equation of state. The top panel shows all experimental data and the bottom panel omits the data of Hirata et al. [34] and Haccuria and Mathieu [31] for clarity

scattered within 1 %. The high-temperature region ($T > 375$ K) was only investigated by Zernov et al. [23], Hirata et al. [34], and de Loos et al. [26]. The data of Zernov et al. [23] deviate by more than 10 % in the region where other data are available. de Loos et al. [26] report that Zernov et al. [23] "did not use an inhibitor to prevent polymerization", which might explain this offset. Therefore, the data of Zernov et al. [23] were not further considered for the fit. Hirata et al. [34] applied two different experimental methods. The first set ("constant pressure method") is significantly scattered, whereas the second set ("constant temperature method") is rather consistent, *cf.* Figure 5. The data of de Loos et al. [26] were measured with a self-made Cailletet apparatus. Since they do not report the original measurements but rather smoothed values, these data were not considered for the adjustment of the present equation of state. Instead, the data of Hirata et al. [34] were chosen. They are

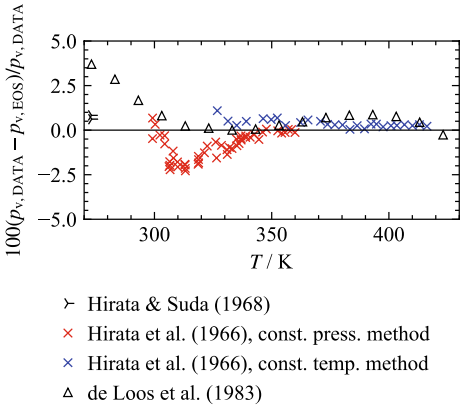

Fig. 5 Percentage deviations of the experimental vapor-pressure data of Hirata and Suda [33], Hirata et al. [34], and de Loos et al. [26] from the equation of state

represented within 0.3 %, which also leads to a reproduction of the data of de Loos et al. [26] within 0.6 % in this temperature region.

The low-temperature region ($T<250$ K) is mainly covered by the data of Haccuria and Mathieu [31] and McDonald et al. [38] except for four other authors with only two state points each. The data of Haccuria and Mathieu [31] significantly differ from other measurements in the medium temperature region and were, therefore, not used in the fitting procedure at low temperatures. The data of McDonald et al. [38] are part of a huge compilation of vapor-pressure data for various fluids. They are reproduced by the present equation of state within 0.35 % except for one outlier. This is in line with what was observed for data for, e.g., ethylene oxide from the same compilation (*cf.* Thol et al. [60]).

Since there is no information on the experimental uncertainty of the measurements available, a reliable statement on the uncertainty of vapor pressures calculated with the present equation of state cannot be made. Simply based on the percentage deviations, the estimated uncertainty is 1%, but might be lower in certain regions.

4.3 Density

The homogeneous density region was investigated in three publications. The single state point of Hayduk and Laudie [49] at 273.15 K is located in the gaseous region and reproduced by the present equation of state within 0.06 %. The data of Cullick and Ely [14] and Javed et al. [12] were measured in overlapping temperature and pressure ranges. They match very well within their experimental uncertainties, see Fig. 6. Since the data of Javed et al. [12] cover broader temperature and pressure ranges, they were used for the development of the present equation of state. They were measured with a vibrating tube densimeter between 283 K and 363 K with a maximum pressure of 91 MPa. The experimental uncertainty is stated to be between 0.11 % and 0.15 % ($k=2$) with the higher uncertainties at low pressures. The present equation of state reproduced the data well within the experimental uncertainty (AARD = 0.046 %).

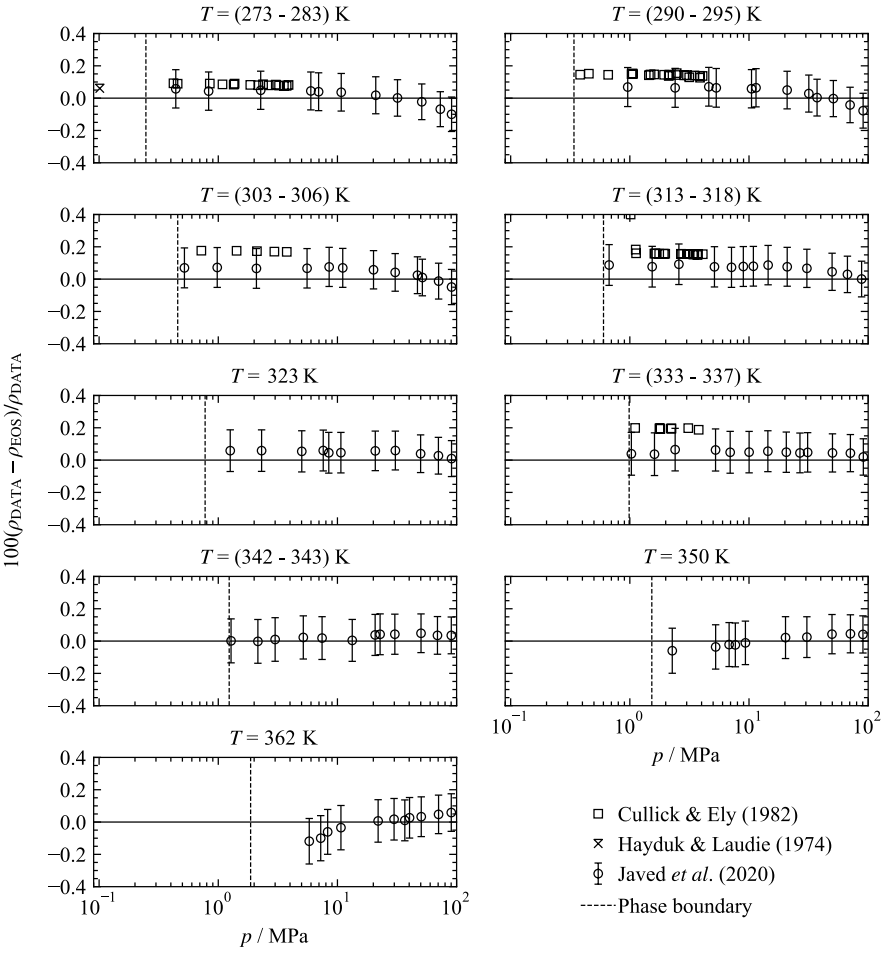

Fig. 6 Percentage deviations of the experimental homogeneous density data from the equation of state as a function of pressure separated into temperature ranges. The vertical dashed lines are the vapor pressures evaluated at the temperatures at which the data of Javed et al. [12] were measured. The experimental uncertainties are shown with error bars

In addition to the homogeneous density, there are five datasets available for the saturated liquid density, *cf.* Table 6. Except for the data of de Loos et al. [26], all data agree within 0.4 % (see top panel of Fig. 7) although saturated liquid density data were not used to adjust the parameters. The most recent state point of Zerfa and Brooks [47] is reproduced within 0.026 %, which independently confirms the representation of the data of Javed et al. [12]. In the bottom panel of Fig. 7, the location of the saturated liquid density data in relation to the homogeneous density data is illustrated. The temperature and pressure ranges of the data of Javed et al. [12] overlap with the data of de Loos et al. [26], Dana et al. [25], and Zerfa and Brooks [47]. This clearly shows that the data of de Loos et al. [26] exhibit a systematic offset to

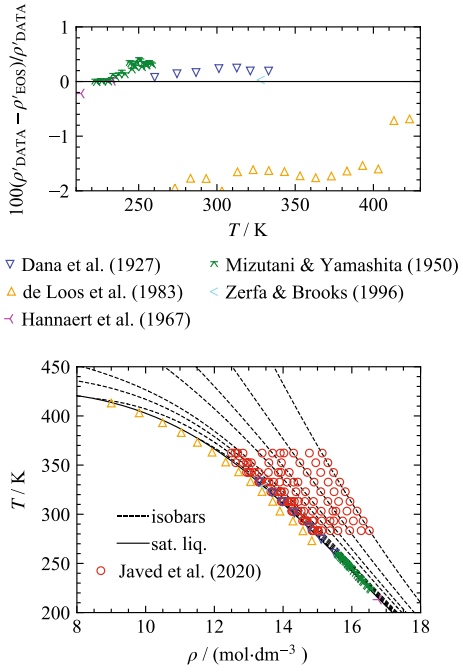

Fig. 7 Percentage deviations of the experimental saturated liquid density data from the equation of state (top) and a T,ρ-diagram showing the distribution of the homogeneous density data of Javed et al. [12] and the saturated liquid density data (bottom)

all other data and are, therefore, not further considered for the evaluation of the present equation of state even in the higher temperature range where no other data are available. The low-temperature data of Mizutani and Yamashita [48] and Hannaert et al. [32] are consistent with the data of Dana et al. [25] with just a small offset.

Based on the discussion above, the uncertainty of liquid densities calculated with the present equation of state is expected to be 0.15 % ($k=2$) at temperatures between 210 K and 365 K with pressures up to 100 MPa. Due to the incomplete database, no statement can be made about the uncertainty in the gaseous phase.

4.4 Speed of Sound

There is only one dataset available for the speed of sound of vinyl chloride. It was recently published by Javed et al. [12] and comprises 117 state points in the liquid state between 283 K and 362 K with a maximum pressure of 91 MPa. Since it is the only comprehensive dataset in the literature providing information on caloric properties of this fluid, it was very important for the development of the present equation of state. The data were measured with two different apparatuses based on the pulse-echo method. Except for one state point, the experimental uncertainty is less than 0.15 % ($k=2$). Figure 8 shows that all data are represented well within the experimental uncertainty (AARD = 0.032 %). Therefore, the uncertainty of the equation of state is also expected to be 0.15 % ($k=2$) in the corresponding temperature and pressure range.

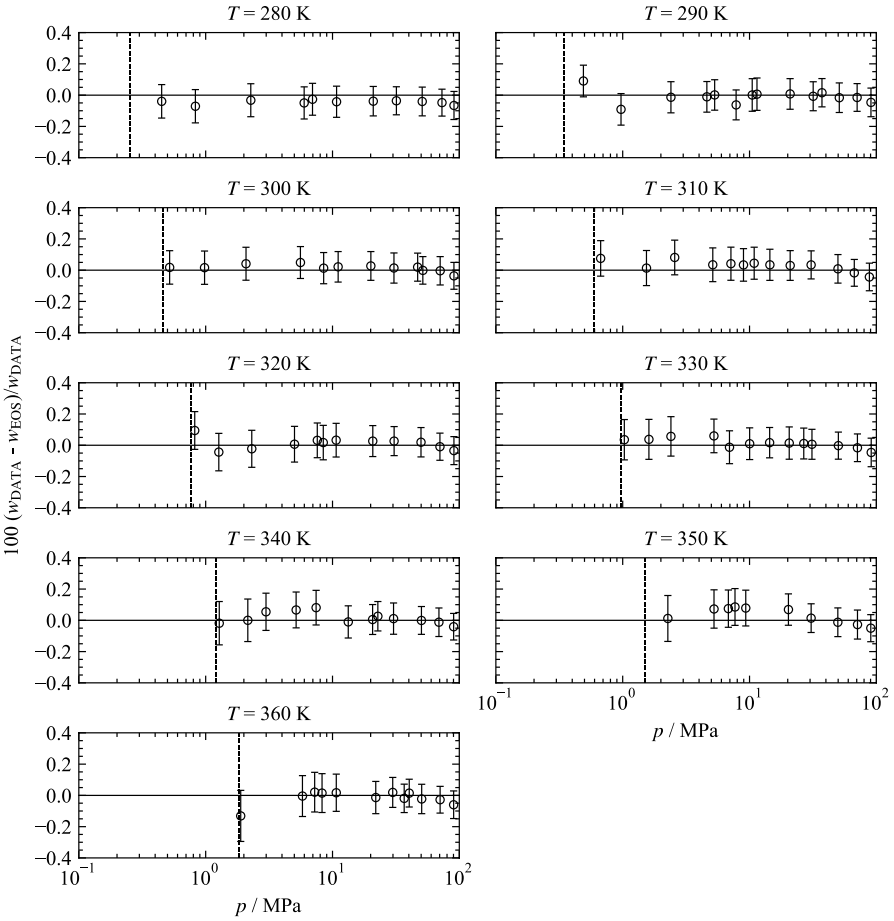

Fig. 8 Percentage deviations of the experimental speed-of-sound data of Javed et al. [12] from the equation of state as a function of pressure along isotherms. The vertical dashed lines are the vapor pressures evaluated at the temperatures at which the data of Javed et al. [12] were measured. The experimental uncertainties are shown with error bars

5 Physical Behavior of the Equation of State

In addition to reproducing the experimental data as accurately as possible, it is important to ensure correct physical behavior of the equation of state in areas where no data are available. This aspect is especially important for fluids, such as vinyl chloride, for which experimental data are very limited. Moreover, the use of the pure-fluid equation in mixture models makes a reasonable extrapolation behavior essential, since a mixture state point may be evaluated outside the ranges of validity of the corresponding pure-fluid equations.

The physical behavior of an equation of state is constantly monitored during the fitting procedure. For this purpose, many different thermodynamic properties

are analyzed in absolute diagrams. While the analysis of thermal properties has been standard for a long time, caloric properties are now also of great importance. Common caloric properties used in the evaluation are the heat capacity and speed of sound, but also less known quantities, such as the phase identification parameter [61] or Grüneisen parameter [62]. While the last two properties are mostly irrelevant for the real application of fluid equations of state, they are very helpful in the fitting process. They not only combine thermal and caloric state variables, but are composed of higher derivatives of the Helmholtz energy with respect to their independent variables. This allows for the detection of unreasonable behavior in order to effectively correct the equation of state for higher orders of derivatives. More detailed information on the analysis of the physical behavior of equations of state is given in Refs. [10, 13, 63–65].

Example plots showing the correct physical behavior of the present equation of state are illustrated in Fig. 9. The top left panel shows smooth behavior of the thermal properties including a distinct saddle point, $(\partial p/\partial \rho)_{T_c} = 0$ and $\left(\partial^2 p/\partial \rho^2\right)_{T_c} = 0$, of the critical isotherm at the critical point. The top right panel demonstrates the correct behavior at extreme temperatures ($T_{\max} = 10^6$ K), pressures, and densities with isotherms converging but not crossing each other. Figure 9c and d depict the residual isochoric heat capacity ($c_v^{\mathrm{r}} = c_v - c_v^{\mathrm{o}}$) and the speed of sound, respectively. Characteristic features are the positive curvature of the residual isochoric heat capacity in the liquid phase with a negative slope at very low temperatures changing to a positive slope while approaching the critical temperature. The saturated gaseous phase exhibits a positive slope and curvature over the entire temperature range, crosses the saturated liquid curve, and matches the saturated liquid curve at a distinct maximum. In line with this, the speed of sound exhibits a pronounced minimum at the critical point. The saturated liquid curve has a negative slope, whereas the saturated vapor curve shows a change from a positive to a negative slope with increasing temperatures while maintaining negative curvature. In the bottom panels, the phase identification [61] and the residual Grüneisen parameters are illustrated. The phase identification parameter [61] (Fig. 9e) exhibits a positive slope and curvature along the saturated liquid curve, whereas the saturated vapor curve has a negative slope and curvature. The residual Grüneisen parameter is defined as $\Gamma^{\mathrm{res}} = (\partial p/\partial T)_\rho / \left(\rho c_v^{\mathrm{r}}\right)$. The trend of the residual Grüneisen parameter (Fig. 9f) is quite similar to the speed of sound. The only relevant difference is that isobars should have a negative curvature at temperatures below the critical temperature.

Finally, the so-called ideal curves (*cf.* Span and Wagner [66]) and the thermal virial coefficients are presented in Figs. 10 and 11. Correct behavior of thermal properties is indicated by smooth courses of the ideal curves without any unreasonable change in slopes or curvatures as visible in Fig. 10.

The correct behavior of the virial coefficients is not yet exactly known. However, for simple monatomic fluids, Thol et al. [64] showed some characteristics by means of statistical mechanics that should be fulfilled. Although vinyl chloride is a more complex molecule, it does not have strong electrostatic interactions and is, therefore, expected to behave similarly. This is confirmed by Fig. 11. All virial coefficients go to

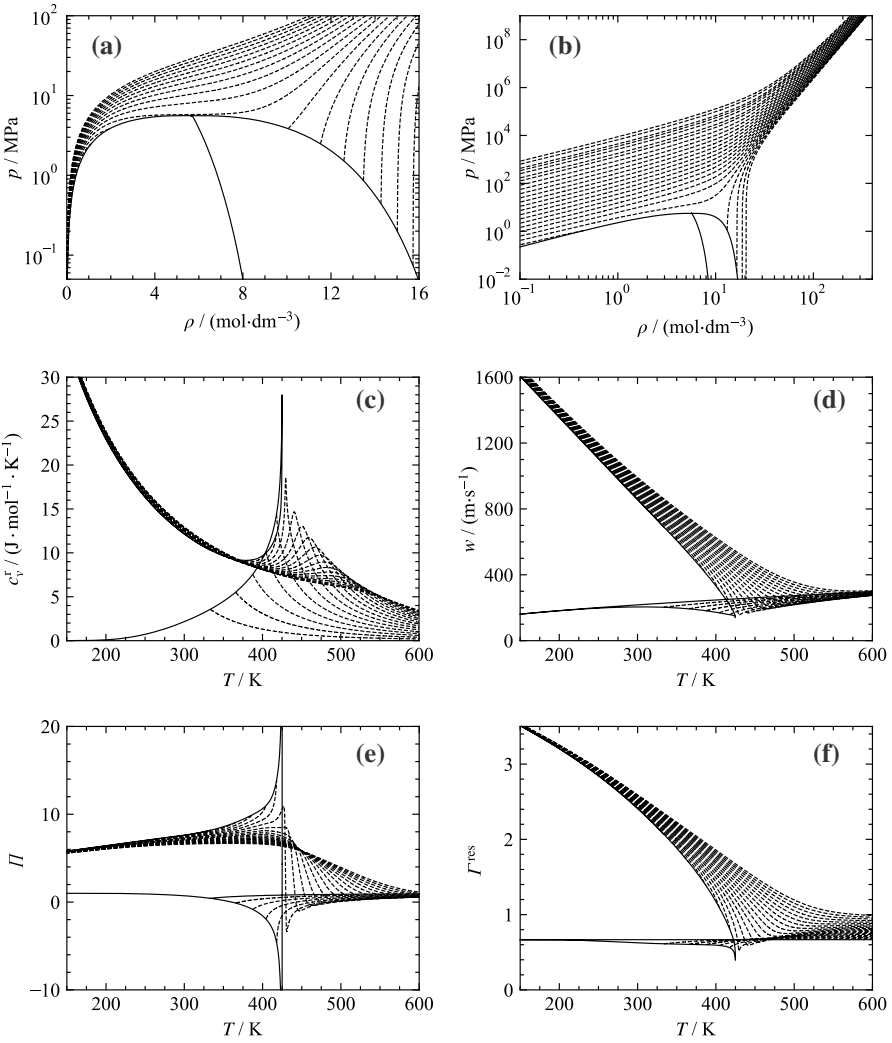

Fig. 9 Exemplary plots of thermodynamic properties, which are investigated during the fitting process in order to ensure physically correct behavior of the equation of state: (a) p,ρ-diagram along isotherms, (b) double-logarithmic p,ρ-diagram along isotherms ($T_{max} = 10^6$ K), (c) c_v^r,T-diagram along isobars, (d) w,T-diagram along isobars, (e) Π,T-diagram along isobars, and (f) Γ^{res},T-diagram along isobars

negative infinity at very low temperatures, exhibit a positive slope and negative curvature, cross the zero line, and decrease until reaching zero without becoming negative again. The distinct maximum of the third and fourth virial coefficients is around the critical temperature. The third virial coefficients should have an inflection point after the maximum. In the case of vinyl chloride, this is too distinct because there is a slight second bump instead. However, this is only barely visible. The less pronounced second bump of the fourth virial coefficient is correct according to Thol et al. [64].

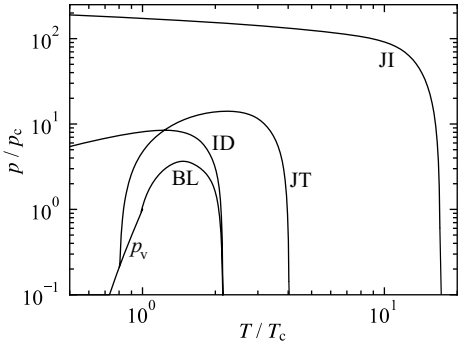

Fig. 10 Characteristic ideal curves according to Span and Wagner [66]. p_v: vapor-pressure curve; BL: Boyle-curve; ID: ideal curve; JT Joule–Thomson inversion curve; JI: Joule inversion curve

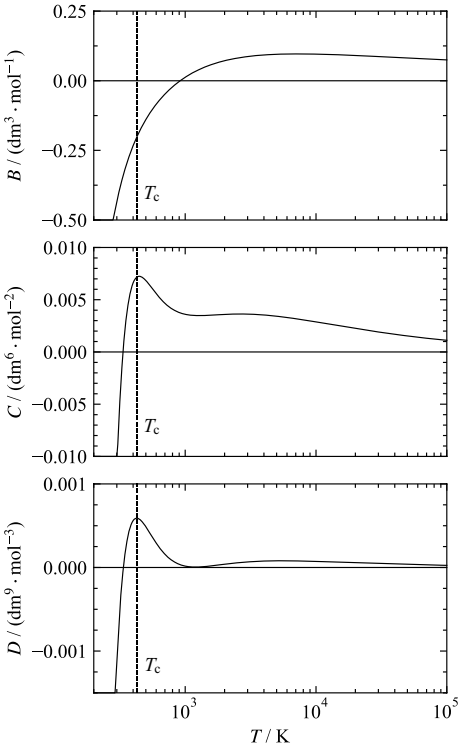

Fig. 11 Second (top), third (center), and fourth (bottom) thermal virial coefficients as functions of temperature

In summary, Figs. 9, 10, 11 demonstrate correct physical behavior of the present equation of state, which ensures that this equation can be applied to mixtures models.

6 Conclusion

A fundamental equation of state in terms of the Helmholtz energy was developed for vinyl chloride. It can be used to calculate all thermodynamic state properties through the combination of its derivatives with respect to the independent variables temperature and density. The experimental database is rather limited and thus the range of validity only covers temperatures of 119.31 K to 430 K with a maximum pressure of 100 MPa. The lowest temperature where experimental data are available is significantly higher than the triple-point temperature of vinyl chloride. Therefore, uncertainty statements can only be made for temperatures above 190 K. However, reliable extrapolation down to low temperatures is ensured. The parameters of the equation were adjusted to vapor-pressure, homogeneous density, and speed-of-sound data, resulting in expected uncertainties ($k=2$) of calculated values in the region where experimental data are available of 1 %, 0.15 %, and 0.15 %, respectively.

Due to the restricted database, it is important to ensure the physically correct behavior of the equation of state. For this purpose, several constraints were applied to the fit. In this way, all demands on the physical behavior of modern equations of state are fulfilled. The present equation can be used in the mathematical framework of Helmholtz mixture equations such as the GERG-2008 [67], EOS-CG [68], or EOS-LNG [69]. This is an important basis for more accurate simulation of processes in the chemical industry involving vinyl chloride, for example, the production of polyvinyl chloride.

7 Supporting Information Available

A text file containing the parameters of the equation is available. For the use in REFPROP [6] or TREND [70], it must be renamed as vinylchloride.fld.

Funding Open Access funding enabled and organized by Projekt DEAL.

References

1. E.-L. Dreher, K.K. Beutel, J.D. Myers, T. Lübbe, S. Krieger, L.H. Pottenger, in *Ullmann's Encyclopedia of Industrial Chemistry*, ed. by B. Elvers and F. Ullmann (Wiley-VCH Verlag GmbH & Co. KGaA, Weinheim, Germany, 2011), p. 1–81.

2. Occupational Safety and Health Administration (OSHA), *1910.1017—Vinyl chloride* (Washington, D.C., USA, 1993).
3. R.J. Waxweiler, W. Stringer, J.K. Wagoner, J. Jones, H. Falk, C. Carter, Ann. N. Y. Acad. Sci. **271**, 40–48 (1976)
4. National Center for Biotechnology Information, *PubChem—Vinyl chloride*. https://pubchem.ncbi.nlm.nih.gov/compound/6338. Accessed 15 October 2021.
5. K. Gao, J. Wu, E.W. Lemmon, *Helmholtz equation of state for acetylene* (to be published, 2022).
6. E.W. Lemmon, I.H. Bell, M.L. Huber, M.O. McLinden, *NIST Standard Reference Database 23: Reference Fluid Thermodynamic and Transport Properties-REFPROP, Version 10.0* (National Institute of Standards and Technology, Gaithersburg, USA, 2018).
7. M. Thol, F.H. Dubberke, E. Baumhögger, R. Span, J. Vrabec, J. Chem. Eng. Data **63**, 2533–2547 (2018)
8. M. Thol, G. Rutkai, A. Köster, W. Wagner, R. Span, J. Vrabec, Mol. Phys. **115**, 1166–1185 (2017)
9. M. Thol, S. Herrig, R. Span, E.W. Lemmon, AIChE J. **e17326** (2021).
10. E.W. Lemmon, R.T. Jacobsen, J. Phys. Chem. Ref. Data **34**, 69–108 (2005)
11. E.W. Lemmon, *Numerical Fitting Algorithm for the Development of Equations of State* (personal communication, 2020).
12. M.A. Javed, M. Rüther, E. Baumhögger, J. Vrabec, J. Chem. Eng. Data **65**, 2495–2504 (2020)
13. R. Span, *Multiparameter Equations of State: An Accurate Source of Thermodynamic Property Data* (Springer, Berlin, 2000)
14. A.S. Cullick, J.F. Ely, J. Chem. Eng. Data **27**, 276–281 (1982)
15. B.V. Lebedev, I.B. Rabinovich, V.A. Budarina, Polym. Sci. USSR **9**, 545–552 (1967)
16. M.E. Wieser, M. Berglund, Pure Appl. Chem. **81**, 2131–2156 (2009)
17. E. Tiesinga, P.J. Mohr, D.B. Newell, B.N. Taylor, Rev. Mod. Phys. **93**, 025010 (2021)
18. W. Wagner, *Eine thermische Zustandsgleichung zur Berechnung der Phasengleichgewichte flüssig-gasförmig für Stickstoff*. Ph.D. Dissertation (Braunschweig, 1970).
19. W. Wagner, Cryogenics **12**, 214–221 (1972)
20. D. Ambrose, J. Chem. Thermodyn. **10**, 765–769 (1978)
21. D. Ambrose, J. Counsell, C. Hicks, J. Chem. Thermodyn. **10**, 771–778 (1978)
22. R.C. Reid, J.M. Prausnitz, T.K. Sherwood, *The Properties of Gases and Liquids* (McGraw-Hill, New York, 1977)
23. V.S. Zernov, V.B. Kogan, S.G. Lyubetskii, V.M. Kobyakov, Viniti Code **1479–78**, 1–11 (1978)
24. S. Carra, P. Beltrame, Chim. Ind. **43**, 1251–1254 (1961)
25. L.I. Dana, J.N. Burdick, A.C. Jenkins, J. Am. Chem. Soc. **49**, 2801–2806 (1927)
26. T.W. de Loos, H.J. van der Kooi, W. Poot, P.L. Ott, Delft Progress Report **8**, 200–213 (1983)
27. R.R. Dreisbach, S.A. Shrader, Ind. Eng. Chem. **41**, 2879–2880 (1949)
28. N.F. Giles, G.M. Wilson, J. Chem. Eng. Data **51**, 1973–1981 (2006)
29. P.C. Gillespie, J.R. Cunningham, G.M. Wilson, AIChE Symp. Ser. **81**, 49–56 (1985)
30. P.C. Gillespie, J.R. Cunningham, G.M. Wilson, AIChE Symp. Ser. **81**, 57–64 (1985)
31. M. Haccuria, M.P. Mathieu, Ind. Chim. Belge **32**, 165–167 (1967)
32. H. Hannaert, M. Haccuria, M.P. Mathieu, Ind. Chim. Belge **32**, 156–164 (1967)
33. M. Hirata, S. Suda, Bull. Jpn. Petrol. Inst. **10**, 20–27 (1968)
34. M. Hirata, S. Suda, H. Sagara, Sekiyu-gakkai-shi **9**, 712–722 (1966)
35. G. Hradetzky, M. Mühlenbruch, I. Richter, Chem. Prum. **26**, 31–33 (1976)
36. A. Kováč, J. Dykyj, Petrochemia **11**, 91–93 (1971)
37. J.S. Lim, Y.-W. Lee, Y.Y. Lee, J. Chem. Eng. Data **42**, 566–569 (1997)
38. R.A. McDonald, S.A. Shrader, D.R. Stull, J. Chem. Eng. Data **4**, 311–313 (1959)
39. J.L. Owens, J. Brady, J.R. Freeman, W.V. Wilding, G.M. Wilson, AIChE Symp. Ser. **83**, 18–41 (1987)
40. C.R. Pearson, G. McConnell, R.B. Cain, Proc. R. Soc. Lond. B **189**, 305–332 (1975)
41. R. Pelnar, Chem. Prum. **10**, 308–310 (1960)
42. H. Preuss, K. Moerke, *Leuna Protocol 10091* (Leuna-Merseburg, Germany, 1987)
43. H. Preuss, K. Moerke, *Leuna Protocol 11271* (Leuna-Merseburg, Germany, 1987)
44. H. Preuss, K. Moerke, *Leuna Protocol 5101* (Leuna-Merseburg, Germany, 1988)
45. H. Preuss, T. Roscher, *Leuna Protocol 6261* (Leuna-Merseburg, Germany, 1973)
46. S.I. Rozloskaya, M.I. Temkin, Zh. Prikl, Khim. **19**, 30–34 (1946)
47. M. Zerfa, B.W. Brooks, Chem. Eng. Sci. **51**, 3223–3233 (1996)
48. K. Mizutani, K. Yamashita, J. Natl. Chem Labor **45**, 49–56 (1950)

49. W. Hayduk, H. Laudie, J. Chem. Eng. Data **19**, 253–257 (1974)
50. H. Senftleben, Z. Angew, Phys. **5**, 33–39 (1953)
51. R.M. Joshi, B.J. Zwolinski, J. Polym. Sci. B Polym. Lett. **3**, 779–781 (1965)
52. S.M. Danov, Y.D. Golubev, Tr. Khim. Khim. Tekhnol. 52–55 (1967).
53. C.W. Gullikson, J. Nielsen, J. Mol. Spectrosc. **1**, 158–178 (1957)
54. J.R. Lacher, E. Emery, B. Bohmfalk, J.D. Park, J. Phys. Chem. **60**, 492–495 (1956)
55. R.E. Richards, J. Chem. Soc., 1931–1933 (1948).
56. H. Senftleben, Z. Angew, Physics **17**, 86–87 (1964)
57. R.T. Birge, Rev. Mod. Phys. **13**, 233–239 (1941)
58. J.O. Hirschfelder, J. Chem. Phys. **8**, 431–432 (1940)
59. H.W. Thompson, P. Torkington, Proc. R. Soc. Lond. A **184**, 3–20 (1945)
60. M. Thol, G. Rutkai, A. Köster, M. Kortmann, R. Span, J. Vrabec, Chem. Eng. Sci. **121**, 87–99 (2015)
61. G. Venkatarathnam, L.R. Oellrich, Fluid Phase Equilib. **301**, 225–233 (2011)
62. V.D. Arp, J.M. Persichetti, G. Chen, J. Fluids Eng. **106**, 193–201 (1984)
63. E.W. Lemmon, M.O. McLinden, W. Wagner, J. Chem. Eng. Data **54**, 3141–3180 (2009)
64. M. Thol, G. Rutkai, A. Köster, R. Span, J. Vrabec, R. Lustig, J. Phys. Chem. Ref. Data **45**, 023101 (2016)
65. S. Herrig, M. Thol, A.H. Harvey, E.W. Lemmon, J. Phys. Chem. Ref. Data **47**, 043102 (2018)
66. R. Span, W. Wagner, Int. J. Thermophys. **18**, 1415–1443 (1997)
67. O. Kunz, W. Wagner, J. Chem. Eng. Data **57**, 3032–3091 (2012)
68. J.G. Gernert, R. Span, J. Chem. Thermodyn. **93**, 274–293 (2016)
69. M. Thol, M. Richter, E.F. May, E.W. Lemmon, R. Span, J. Phys. Chem. Ref. Data **48**, 33102 (2019)
70. R. Span, R. Beckmüller, S. Hielscher, A. Jäger, E. Mickoleit, T. Neumann, S. Pohl, B. Semrau, M. Thol, *TREND. Thermodynamic Reference and Engineering Data 5.0* (Lehrstuhl für Thermodynamik, Ruhr-Universität Bochum, Bochum, Germany, 2020).